



# An effective and accessible cell configuration for testing rechargeable zinc-based alkaline batteries

Yamin Zhang<sup>a,1</sup>, Yifan Zhang<sup>b,1</sup>, Anmol Mathur<sup>a</sup>, Sarah Ben-Yoseph<sup>a</sup>, Song Xia<sup>a</sup>, Yutong Wu<sup>a</sup>, Nian Liu<sup>a,\*</sup>

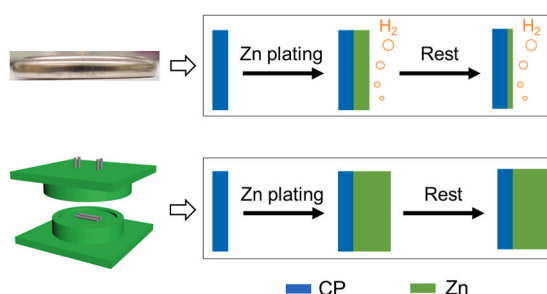
<sup>a</sup> School of Chemical and Biomolecular Engineering, Georgia Institute of Technology, Atlanta, GA, 30332, USA

<sup>b</sup> School of Chemistry and Biochemistry, Georgia Institute of Technology, Atlanta, GA, 30332, USA

## HIGHLIGHTS

- The electrochemical cell–gas chromatography analysis method was setup.
- 99% of the capacity loss on the zinc anode was caused by the HER.
- The testing device has a clear effect on the HER in alkaline zinc batteries.
- HER and self-discharge of Zn were visualized through operando optical microscopy.
- An effective and accessible cell configuration was designed to minimize HER.

## GRAPHICAL ABSTRACT



## ARTICLE INFO

### Keywords:

Zinc anode  
Hydrogen evolution  
Aqueous  
Alkaline electrolyte  
Corrosion  
Cell configuration

## ABSTRACT

Rechargeable aqueous zinc–air batteries have received much attention due to their intrinsic safety, high theoretical volumetric energy density (6134 Wh/L), and low cost. However, zinc anodes suffer from severe hydrogen evolution reaction (HER) in alkaline electrolytes, which are kinetically favorable for air cathodes. Through an electrochemical cell–gas chromatography setup, we quantitatively identified that 99% of the capacity loss on the zinc anode was caused by HER. Most previous research has focused on material design to suppress HER, while less attention has been paid to the device. Here we demonstrate that the testing device has an apparent effect on the HER in alkaline electrolytes. Stainless-steel coin cells, as common devices used in research laboratories, accelerate HER due to synergistic effects of galvanic corrosion and a high HER activity. We designed an effective and accessible cell configuration for testing zinc-based alkaline batteries, which minimizes HER and demonstrates a higher Coulombic efficiency and longer cycling life than stainless-steel coin cells. Minimized HER and self-discharge of Zn were visualized through the operando optical microscopy. Specifically, the Ni–Zn battery with our cell configuration achieved stable long-term cycling for 816 cycles compared with ~100 cycles for the stainless-steel cell. The cell configuration shown here can be directly used or modified for future research on zinc-based aqueous batteries.

\* Corresponding author.

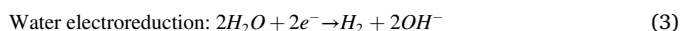
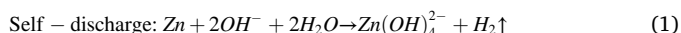
E-mail address: [nian.liu@chbe.gatech.edu](mailto:nian.liu@chbe.gatech.edu) (N. Liu).

<sup>1</sup> These authors contributed equally to this work.

## 1. Introduction

The current power-storage landscape is dominated by lithium-ion batteries (LIBs) [1–3] because they provide a high energy density, high specific power, and long cycle life. However, the volatility and flammability of the organic liquid electrolytes in LIBs are threats to battery safety. A safer alternative energy storage system is batteries with aqueous electrolytes, which generally have a higher intrinsic safety, lower cost, and higher ionic conductivity [4,5]. Zinc is the most active metal anode that is stable in water with a low redox potential (−0.762 V vs. SHE). In addition, zinc has a low toxicity, low cost, high theoretical gravimetric capacity of 820 mA h g<sup>−1</sup>, and high theoretical volumetric capacity of 5854 mA h cm<sup>−3</sup> (vs. 2062 mA h cm<sup>−3</sup> for Li) [6,7]. In particular, Zn-air batteries [8] possess a high theoretical volumetric energy density of 6134 Wh/L. Primary Zn-air batteries are already commercially available for high-value and low-mass applications such as hearing aids, but rechargeable ones are not yet ready for commercialization.

Zinc anodes can function in both alkaline and neutral/mild acidic electrolytes. However, only alkaline electrolytes are kinetically favorable for air cathodes [9]. Thus, to develop rechargeable zinc-air batteries, it is essential to enable the use of rechargeable zinc anodes in alkaline electrolytes despite the resulting worse rechargeability and cyclability compared with those in neutral electrolytes. Zinc anodes suffer from passivation, shape change, and dendrite growth in alkaline electrolytes, which have recently been addressed to some extent [10–13]. However, the hydrogen evolution issue remains the main cause of the low Coulombic efficiency (CE) of zinc-based alkaline batteries. Hydrogen evolution follows two reactions: self-discharge of zinc (Reaction (1) or (2)), electrons directly from the external circuit and water electroreduction (Reaction (3)). Zinc is active in alkaline electrolytes and can thus react with them, which is known as self-discharge and decreases the shelf life of zinc batteries. Water electroreduction is a thermodynamically favored side reaction on the zinc anode during charging. The hydrogen gas evolved from these two reactions will dry the electrolyte and cause cell failure and even battery explosion.



The hydrogen evolution reaction (HER) is a general problem for all aqueous battery anodes, which is of significant research interest. Over the years, in order to suppress the HER on zinc anodes, much research has been performed, resulting in approaches including anode surface treatments [14,15] and additives [16,17]. Most of these previous studies focused on material design to improve zinc anodes. However, less attention has been paid to the device level, which is demonstrated in this study to have an apparent effect on the HER in alkaline electrolytes. Coin cells made of stainless-steel (SS) are widely used in research laboratories for zinc-based alkaline batteries [18–27] with the benefits of being small, fast and easy to assemble, and requiring small amounts of active materials. However, we discovered that the coin cell case made of SS accelerates the HER on Zn anodes due to the synergistic effects of galvanic corrosion and a high HER activity, which cause a low CE and short cycling life for zinc-based batteries. Ni-coated steel [28] is widely used in Ni-metal hydride and Ni–Cd rechargeable batteries based on alkaline electrolytes. However, Ni and some of its alloys are amongst the active electrode materials for HER in alkaline solutions [29,30]. We have demonstrated in this study that Ni-coated steel is not a good candidate for testing Zn-based alkaline batteries. Even though the Sn-coated SS case [26] has been reported to suppress the HER, Sn metal corrodes [31] gradually in the alkaline electrolyte. Thus, SS will still be exposed to the electrolyte over the time.

Through an electrochemical cell–gas chromatography setup, we

quantitatively identified that 99% of the capacity loss on the zinc anode was caused by HER, which has not been reported before. We then concluded that the HER is the main side reaction occurring on the zinc anode. In other words, a high-Coulombic-efficiency zinc anode can be achieved by minimizing the HER. Herein, we designed the plastic cell case, an effective and accessible cell configuration for testing zinc-based alkaline batteries, which minimizes the HER, improves the electrochemical performance of zinc anodes, and demonstrates a higher Coulombic efficiency and longer cycling life than stainless-steel coin cells. As visualized through the operando optical microscopy, the HER and the self-discharge of Zn are minimized using the plastic cell case compared to SS cell case. Our research shown in this study quantitatively identified the contribution of HER on the capacity loss of Zn anodes, and would provide researchers with insights into the choice of proper testing devices and current collectors for Zn-based alkaline batteries. In addition, the plastic case is small, easy to fabricate and assemble, and only requiring small amounts of active materials and electrolytes. The cell configuration shown here can be directly used or modified for future research on zinc-based aqueous batteries.

## 2. Experiment section

### 2.1. Material characterization and measurements

The morphological analyses were carried out using scanning electron microscopy (SEM, Hitachi SU 8230). Operando analyses and cyclic voltammetry were conducted using a VSP system (BioLogic). Battery cycling tests were carried out using LANHE operated in galvanostatic mode. In the electrochemical cell–gas chromatography (GC) setup, an airtight battery system was connected to a GC with a thermal conductivity detector (TCD) (MG#5, SRI Instruments), and the system was purged with Ar before measurements. A stainless-steel (SS) rod was used as the anode and ZnO-saturated 4 M KOH (Sigma Aldrich) as the electrolyte. A 4 cm<sup>2</sup> cathode from a commercial Ni–Zn AA battery (PowerGenix), which is a mixture of NiOOH (~8 mA h/cm<sup>2</sup>) and Ni(OH)<sub>2</sub> (~32 mA h/cm<sup>2</sup>), was harvested to pair with the anode. The battery was charged at 20 mA for 15 min and then fully discharged (20 mA) to 0.8 V for 1 cycle. Then, H<sub>2</sub> and O<sub>2</sub> measurements were conducted using the GC-TCD with Ar as the carrier gas. The calculation details can be found in Table S1.

### 2.2. Operando optical microscopy characterization

Two-electrode electrochemical cells were constructed with the substrate of interest as the working electrode and zinc foil as the counter electrode. A ZnO-saturated 4 M KOH (Sigma Aldrich) aqueous solution was used as the electrolyte. The cells were observed using a Leica DMC2700 microscope with reflected dark-field illumination. Most of the images and videos were captured through an air-immersion objective (Leica N PLAN L 5 × 0.50 BD). All the operando experiments were performed at room temperature and ambient pressure.

### 2.3. Electrochemistry

The carbon paper (CP) and zinc foil anodes were cut to round disks with a diameter of 1 cm. The glass fiber (GE Healthcare, Whatman 10370003) separators were round disks with a diameter of 1.6 cm. The counter electrodes (cathodes) were NiOOH/Ni(OH)<sub>2</sub> harvested from commercial Ni–Zn AA batteries (PowerGenix). In order to specifically focus on the zinc anode, it was paired with a NiOOH/Ni(OH)<sub>2</sub> cathode with excess capacity. The electrolyte was 100 μL of ZnO-saturated 4 M KOH (Sigma Aldrich). CR2032 cases (Kelude) made of 304 SS were used to assemble the SS coin cells. Plastic cell cases made of polytetrafluoroethylene were used to assemble the plastic cells. Ti wires were used as electrode terminals for the plastic cells.

The plastic cells and SS coin cells with CP anodes were

galvanostatically charged to the cut-off voltage of 2 V or a charge capacity of 0.106 or 0.212 mA h/cm<sup>2</sup>, followed by full discharge to 1.2 V. The plastic cells and SS coin cells with zinc foil anodes were galvanostatically discharged/charged to the cut-off voltage of 1.2 V/2 V or a discharge/charge capacity of 0.32 mA h/cm<sup>2</sup>.

### 3. Results and discussion

#### 3.1. SS coin cell case induces severe HER and low CE

To focus on zinc anodes, NiOOH/Ni(OH)<sub>2</sub> cathodes with excess capacity of both NiOOH and Ni(OH)<sub>2</sub> were used to make full Ni–Zn batteries in this study. Therefore, the Coulombic inefficiency of the batteries can be directly correlated to side reactions on the zinc anode. NiOOH/Ni(OH)<sub>2</sub>, a mixture of NiOOH (~8 mA h/cm<sup>2</sup>) and Ni(OH)<sub>2</sub> (~32 mA h/cm<sup>2</sup>), was harvested from the cathode of a commercial Ni–Zn AA battery (PowerGenix) [32,33]. To illustrate the HER problem when using SS coin cell cases, we assembled an SS coin cell with a zinc foil round disk (1-cm diameter) as the anode, NiOOH/Ni(OH)<sub>2</sub> (~0.7 cm<sup>2</sup>) as the cathode, and 100  $\mu$ L of 4 M KOH as the electrolyte. The cell was galvanostatically cycled at 1.27 mA/cm<sup>2</sup> to the cut-off voltage of 1.2 V/2 V or a charge/discharge capacity of 0.32 mA h/cm<sup>2</sup>. The calculation of areal parameters was based on the area of the anode if not otherwise specified. As shown in Fig. 1a and Fig. S1, the SS coin cell gradually expanded over cycling, which indicates that gas accumulated in the sealed battery. After cycling for only 77 h, the cell components (electrodes, spacer, and spring) lost contact due to the cell expansion, which resulted in battery failure. With excess cathode materials in both the charged and discharged states (NiOOH and Ni(OH)<sub>2</sub>), the side reactions (e.g., oxygen evolution) on the cathode should be minimized. Thus, we hypothesize that H<sub>2</sub> is the main gas component that causes cell expansion. To prove our hypothesis, we custom-made an air-tight electrochemical cell with an SS rod anode and excess NiOOH/Ni(OH)<sub>2</sub> cathode (4 cm<sup>2</sup>), which was connected to a gas chromatograph (GC, Fig. 1b). The whole cell was purged with Ar before operation. Then, the cell was charged at 20 mA for 15 min and discharged at 20 mA to a cut-off voltage of 0.8 V in a ZnO-saturated [34] 4 M KOH electrolyte, followed by gas-phase measurement through the GC with a thermal conductivity detector (TCD). It is worth mentioning that there was no initial active material on the anode. During charging, in addition to side reactions, zincate in the electrolyte is electrochemically reduced to zinc on the anode. During discharging, zinc is oxidized back to zincate. As shown in Fig. 1c, H<sub>2</sub> was produced after cycling, while a small amount of O<sub>2</sub> was detected, which, to some extent, proves that severe HER is the

main reason for the SS cell expansion shown in Fig. 1a.

We also quantitatively identified the influence of the HER on the capacity loss of zinc anodes with the above electrochemical cell–GC setup. Fig. S2 shows voltage profiles of the Ni–Zn battery, from which we calculated the capacity loss of the zinc anode by subtracting the discharge capacity from the charge capacity. The amount of H<sub>2</sub> produced from the anode was determined by GC–TCD. The results show that 99% (86.6%/87.8%, Table S1) of the capacity loss of the zinc anode was caused by the HER (Fig. 2a). The other 1% of capacity loss was mainly attributed to the oxidation of Zn metal through reacting with trace O<sub>2</sub> generated from the cathode (oxygen reduction reaction (ORR)). Thus, we conclude that the HER is the main side reaction occurring on the zinc anode. In other words, a high-CE zinc anode can be achieved by minimizing the HER.

To study the effect of the SS coin cell case on the HER, we carried out linear sweep voltammetry (LSV) in a three-electrode electrochemical cell with carbon paper, SS, or Ni-coated SS round disks as the working electrode, Hg/HgO as the reference electrode, a graphite rod as the counter electrode, and 4 M KOH as the electrolyte (Fig. S3). Carbon paper (CP) was used as the anode. The Ni-coated SS was prepared by evaporating Ni to a thickness of ~1  $\mu$ m Ni onto SS (Fig. S4). In addition to SS, Ni-coated SS is widely used in Ni-metal hydride and Ni–Cd rechargeable batteries, and thus was also chosen for comparison. As shown in Fig. 2b, the HER on both SS and Ni-coated SS is more severe (higher current density at a fixed HER potential) than on the CP electrode. In addition, the HER activity of Ni-coated SS is even higher than that of SS. Thus, only SS was chosen as the control sample if not otherwise mentioned. These results indicate that the HER on the SS case is more severe than on the anode. Therefore, the HER on zinc anodes is accelerated by the use of an SS coin cell as the device to test alkaline zinc-based batteries. As a result, SS coin cells show low CEs and short cycle lives.

#### 3.2. Cell configuration design for minimizing HER

To minimize the HER induced by the testing device, we fabricated plastic cell cases made of polytetrafluoroethylene (PTFE, Fig. 3a and Fig. S5). Ti wires were used as electrode terminals because Ti demonstrated the highest Coulombic efficiency for Zn plating among 8 metal candidates (Ag, Au, Cu, Ti, Fe, Pt, Ni and stainless steel), as shown in Fig. S6. The CAD file used to fabricate the casings can be found in Supporting Information. This plastic cell configuration is easy to fabricate and thus accessible. They are also small, easy to assemble, and only requiring small amounts of active materials and electrolytes. We

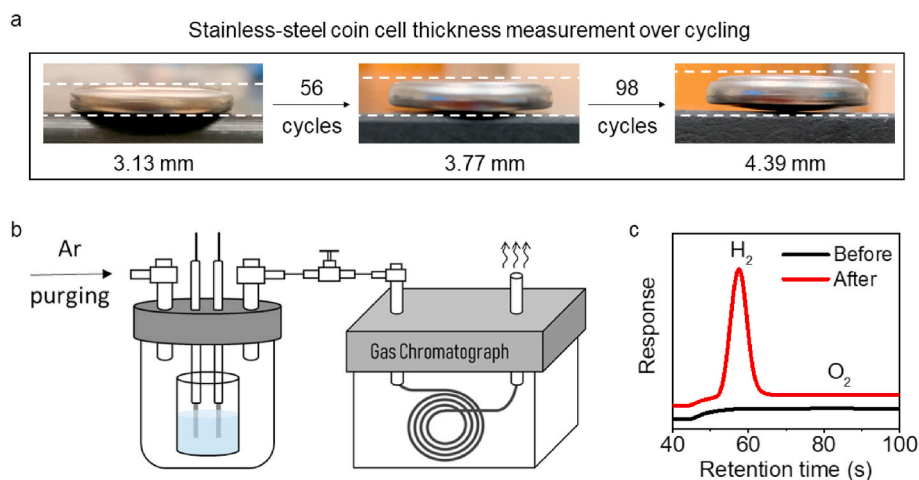


**Fig. 1.** SS coin cell expansion caused by the HER. **a**, Thickness measurement of a Ni–Zn coin cell over cycling with zinc foil as the anode. The coin cell case is SS. **b**, Schematic diagram of the battery–GC quantitative analysis method. **c**, GC–TCD analysis of the gas phase of the Ni–Zn battery before and after cycling in a ZnO-saturated 4 M KOH electrolyte. An SS rod was used as the anode.

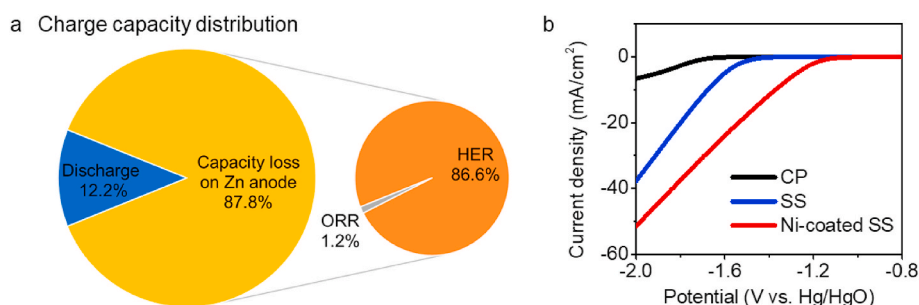


**Fig. 2.** Quantification of the HER and comparison of HER activity. a, Distribution of charge capacity on the anode in the Ni–Zn battery; 99% of the capacity loss on the zinc anode was caused by the HER. b, Linear sweep voltammograms of the CP electrode, SS, and Ni-coated SS in 4 M KOH electrolyte.

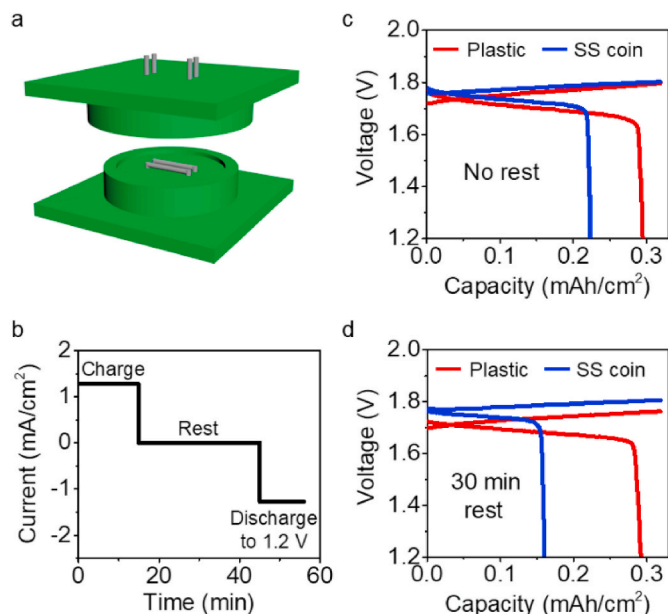


**Fig. 3.** Plastic cell increases the Coulombic efficiency. a, Device fabrication diagram of the plastic cell. b, Current density profiles as cycled under charge–rest–discharge conditions. c,d, Voltage profiles of Ni–Zn batteries tested in both plastic cells and SS coin cells with a rest time of 0 (c) and 30 min (d). CP electrodes were used as anodes.

assembled plastic cells and SS coin cells for comparison containing CP anodes, excess NiOOH/Ni(OH)<sub>2</sub> cathodes, and a ZnO-saturated 4 M KOH electrolyte. The cells were cycled under charge–rest–discharge conditions (Fig. 3b). Specifically, they were galvanostatically charged to the 2 V cut-off voltage or a charge capacity of 0.32 mA h/cm<sup>2</sup>, followed by a rest period (0 or 30 min) and full discharge to 1.2 V. As shown in Fig. 3c and d, plastic cells achieved higher CEs and discharge capacities than the SS coin cells in both rest periods, which demonstrates that the HER can be minimized using a plastic cell device (Fig. 4a). In addition, after 30 min of rest, the CE of the SS coin cells decayed from 70.1% to 50.3%. In contrast, there was only a slight decrease in the CE of the plastic cells from 92.7% to 91.9%. The dramatically decreased CE (~20%) after only 30 min of rest for the SS coin cells indicates that the self-discharge of zinc was accelerated by the SS case, which we believe to be due to galvanic corrosion. During charging, zinc is plated onto both the CP and anode-side SS case. Thus, zinc metal contacts the SS in the electrolyte and corrodes. In other words, the self-discharge of zinc is accelerated (Fig. 4b).

To visualize the HER and self-discharge of zinc in the plastic and SS cells, we conducted operando optical microscopy analysis on CP anodes in the plastic (Fig. 4c, captured from Video S1) and SS (Fig. 4d, captured from Video S2) cells, respectively. Under the same charging conditions,

the HER in the SS cell is more severe than the plastic cell as evidenced by more bubbles and less plated Zn on the CP anode. In addition, the self-discharge of Zn in the SS cell is apparent because Zn corroded and hydrogen formed gradually on the CP anode during the rest period. In addition, we also performed operando visualization [35] of the zinc-plating and resting process on the SS case. As shown in Video S3, numerous bubbles formed along with zinc deposition. This result is in good agreement with our CV analysis showing that the HER is severe on SS [36], which may be due to the presence of nickel [29] in the 304 SS used in this study (Fig. S8). Under resting, Zn corroded severely on the SS case (Fig. S7). Coin cells made of 316 SS also showed a low CE of ~70% (Fig. S9). Thus, when using SS coin cell devices for alkaline zinc-based batteries, the HER will be accelerated by the synergistic effects of galvanic corrosion and the high HER activity of SS. In contrast, the use of non-conductive plastic cells with Ti wires as electrode terminals could minimize the HER.

Supplementary data related to this article can be found at <https://doi.org/10.1016/j.jpowsour.2021.229547>.

### 3.3. Superior cycling performance of plastic cells

The cycling performance of plastic cells and SS coin cells with CP anodes was also tested. Similar to previous experiments, the cells were galvanostatically charged to the cut-off voltage of 2 V or a charge capacity of 0.106 (Fig. 5a) or 0.212 mA h/cm<sup>2</sup> (Fig. 5b), followed by full discharge to 1.2 V. The plastic cells demonstrated a better electrochemical performance than the SS coin cells. When the charge capacity was limited to 0.106 mA h/cm<sup>2</sup>, the plastic cells achieved a higher average CE of 95.1% compared with 74.0% for the SS coin cells. With a charge capacity limit of 0.212 mA h/cm<sup>2</sup>, the plastic cells also exhibited a higher average CE (94.8%) than the SS coin cells (49.8%). Because the CP anodes were cycled at 100% DOD and paired with excess cathode material, the extent of the side reactions occurring on the CP anode can be directly correlated to the cell Coulombic inefficiency. In addition, as discussed above, the HER is the main side reaction on the zinc anode. Thus, we conclude that the high CE of the plastic cells is attributable to the minimized HER on the plastic cell case.

Instead of CP anodes with no loaded active materials, we also galvanostatically cycled both plastic cells and SS coin cells with zinc foil anodes (Fig. 6a). They were discharged/charged to the cut-off voltage of 1.2 V/2 V or a discharge/charge capacity of 0.32 mA h/cm<sup>2</sup>. In the plastic cell, the HER and self-discharge of Zn were minimized (Fig. 6b), thus, the plastic cells achieved stable long-term cycling for 816 cycles compared with ~100 cycles for the SS coin cell. The SS coin cell failure (Fig. 6c) can be attributed to (1) the limited mass transfer of Zn species caused by hydrogen accumulation and electrolyte decomposition, and (2) Zn anode passivation due to the formation of ZnO insulating layer. Voltage profiles of the plastic cells with CP and zinc foil anodes are shown in Figs. S10 and S11. The plastic cell with high areal capacity (~25 mA h/cm<sup>2</sup>) Zn anode also demonstrated a better electrochemical performance than the SS coin cell (Fig. S12). Besides, we tested both CP



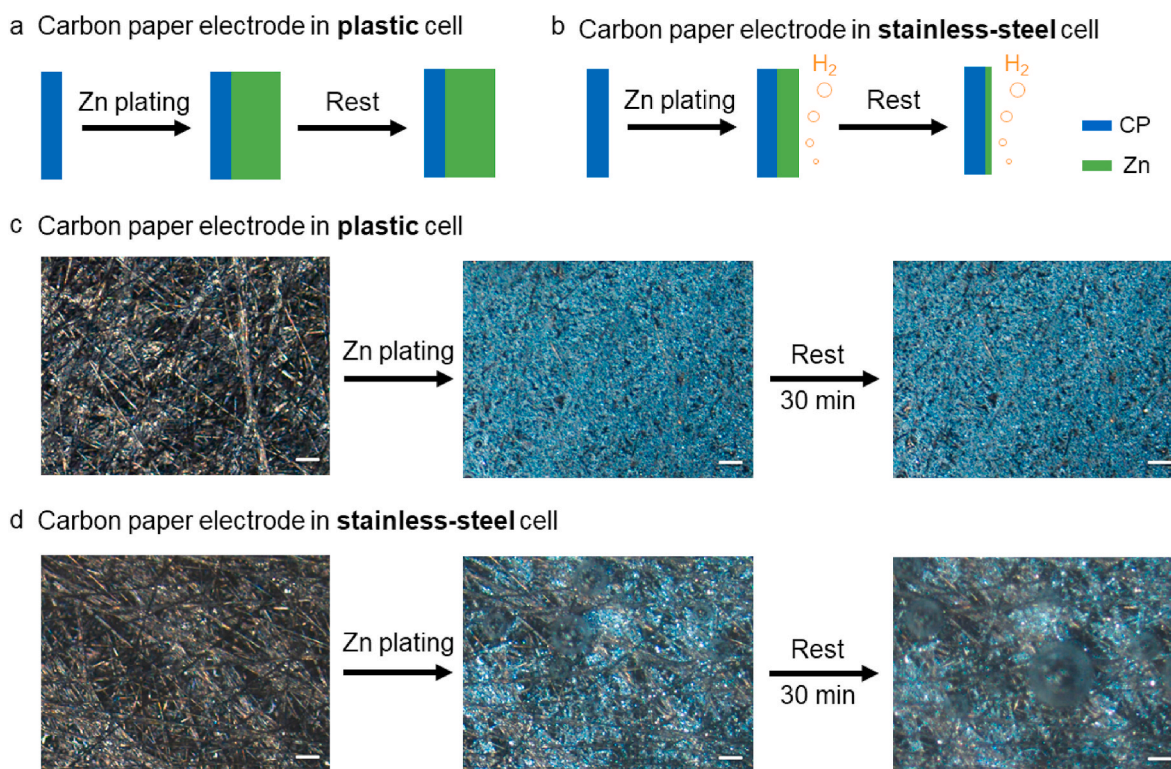


**Fig. 4.** Plastic cell minimizes the self-discharge of Zn anode. a,b, Schematic diagrams of CP electrodes after Zn plating and resting in plastic (a) and stainless-steel (b) cells. c,d, Operando optical microscopy images of CP electrodes after Zn plating and resting in plastic (c) and stainless-steel (d) cells. Electrolyte: ZnO-saturated 4 M KOH. Scale bars: 100  $\mu\text{m}$ .

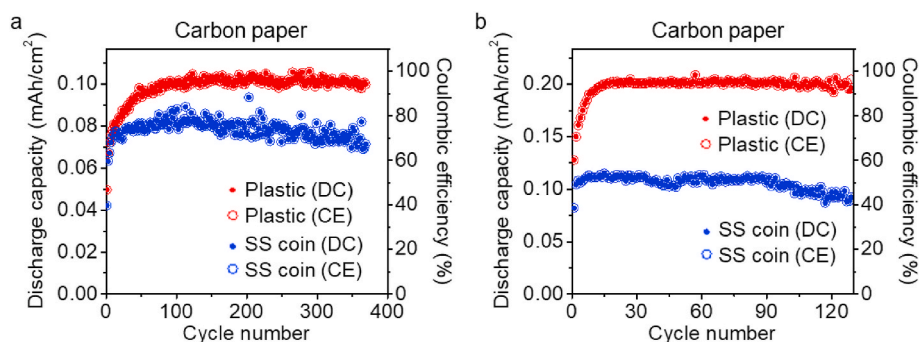


**Fig. 5.** Electrochemical performance of CP electrodes in plastic and SS coin cells. a,b, Cycling performance in ZnO-saturated 4 M KOH electrolyte when galvanostatically charged to the 2 V cut-off voltage or charge capacities of 0.106 (a) and 0.212 mA h/cm<sup>2</sup> (b), followed by full discharge to 1.2 V. Anode current density in all cells: 1.27 mA/cm<sup>2</sup>. DC: discharge capacity. CE: Coulombic efficiency.

anodes and Zn foil anodes in Ni-coated SS coin cells (Fig. S13). Due to the high HER activity [29,30] and severe Zn galvanic corrosion in Ni-coated SS coin cell (Fig. S14), the discharge capacities for both CP anodes and Zn foil anodes were  $\sim 0$  mA h/cm<sup>2</sup>. Voltage profiles of CP and Zn foil anodes in Ni-coated SS cells are shown in Fig. S15.

Instead of PTFE, we also fabricated plastic cell cases using a cheaper material, Delrin. Similarly, the Delrin plastic cells also demonstrated a better electrochemical performance than the SS coin cells (Fig. S16). Thus, even though the battery components were the same, the plastic cells achieved a better electrochemical performance than the SS coin cells. These results reveal that the choice of testing device is important for analyzing zinc-based alkaline batteries. The current cell configuration is designed for testing Ni–Zn batteries, which can be further modified to test Zn–air batteries (Fig. S17). In addition, the structure of the cell can be optimized to minimize material cost and enhance practical relevance (Fig. S18).

#### 4. Conclusion

In this work, through an electrochemical cell–GC setup, we quantitatively identified that 99% of the capacity loss on the zinc anode was caused by the HER. We also demonstrated that the testing device has a notable influence on the HER in alkaline zinc-based batteries. SS coin cells, as widely used devices in research laboratories, accelerate the HER due to the synergistic effects of galvanic corrosion and a high HER activity, which cause a low CE and short cycling life. We designed an effective and accessible cell configuration, plastic cell, for testing zinc-based alkaline batteries. Minimized HER and self-discharge of Zn were visualized through the operando optical microscopy. As a result, the plastic cells demonstrated a higher CE and longer cycling life than the SS coin cells. The cell configuration shown in this work can be directly used or modified for future research on zinc-based aqueous batteries. Our findings also provide insights into choosing proper testing devices for

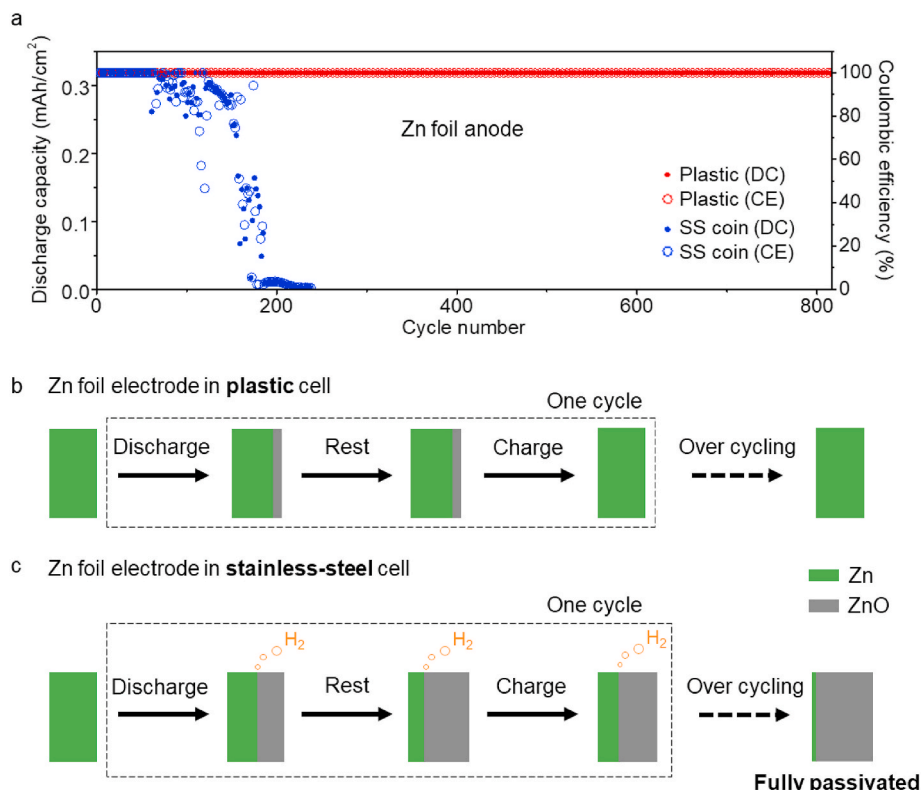


**Fig. 6.** Electrochemical performance of Zn foil anodes in plastic and SS coin cells. a, Cycling performance in a 4 M KOH electrolyte when anodes were galvanostatically discharged/charged to the 1.2 V/2 V cut-off voltage or a discharge/charge capacity of 0.32 mA h/cm<sup>2</sup>. Anode current density in all cells: 1.27 mA/cm<sup>2</sup>. DC: discharge capacity. CE: Coulombic efficiency. b,c, Schematic diagrams of electrodes over cycling in plastic (b) and stainless-steel (c) cells.

zinc-based batteries.

#### Author contributions

Y.Z. and N.L. conceived the idea. Y.Z., Y.Z., and N.L. co-wrote the manuscript. Y.Z. carried out the material characterization and electrochemical measurements. Y.Z., A.M., S.B.Y., S.X. and Y.W. assisted with electrochemical measurements and sample preparation. All authors discussed the results and commented on the manuscript.

#### Declaration of competing interest

The authors declare that they have no known competing financial interests or personal relationships that could have appeared to influence the work reported in this paper.

#### Acknowledgment

N. L. acknowledges support from faculty startup funds from the Georgia Institute of Technology. Dillon Jones and Harper Finch are acknowledged for their experimental supports. The air-tight electrochemical cell and plastic cells were made by the Machine Research Services group in the School of Chemical & Biomolecular Engineering at Georgia Institute of Technology. Material characterization was performed in part at the Georgia Tech Institute for Electronics and Nanotechnology, a member of the National Nanotechnology Coordinated Infrastructure, which is supported by the National Science Foundation (Grant ECCS-1542174).

#### Appendix A. Supplementary data

Supplementary data to this article can be found online at <https://doi.org/10.1016/j.jpowsour.2021.229547>.

#### References

- [1] Y. Zhang, N. Liu, Nanostructured electrode materials for high-energy rechargeable Li, Na and Zn batteries, *Chem. Mater.* 29 (2017) 9589–9604, <https://doi.org/10.1021/acs.chemmater.7b03839>.
- [2] J. Ma, J. Sung, J. Hong, S. Chae, N. Kim, S.-H. Choi, G. Nam, Y. Son, S.-Y. Kim, M. Ko, J. Cho, Towards maximized volumetric capacity via pore-coordinated design for large-volume-change lithium-ion battery anodes, *Nat. Commun.* 10 (2019) 475, <https://doi.org/10.1038/s41467-018-08233-3>.
- [3] N. Liu, G. Zhou, A. Yang, X. Yu, F. Shi, J. Sun, J. Zhang, B. Liu, C.-L. Wu, X. Tao, Y. Sun, Y. Cui, S. Chu, Direct electrochemical generation of supercooled sulfur microdroplets well below their melting temperature, *Proc. Natl. Acad. Sci. Unit. States Am.* 116 (2019) 765–770, <https://doi.org/10.1073/pnas.1817286116>.
- [4] J.-Y. Luo, W.-J. Cui, P. He, Y.-Y. Xia, Raising the cycling stability of aqueous lithium-ion batteries by eliminating oxygen in the electrolyte, *Nat. Chem.* 2 (2010) 760–765, <https://doi.org/10.1038/nchem.763>.
- [5] J. Xie, Q. Zhang, Recent progress in multivalent metal (Mg, Zn, Ca, and Al) and metal-ion rechargeable batteries with organic materials as promising electrodes, *Small* 1805061 (2019) 1805061, <https://doi.org/10.1002/sml.201805061>.
- [6] F. Wang, O. Borodin, T. Gao, X. Fan, W. Sun, F. Han, A. Faraone, J.A. Dura, K. Xu, C. Wang, Highly reversible zinc metal anode for aqueous batteries, *Nat. Mater.* 17 (2018) 543–549, <https://doi.org/10.1038/s41563-018-0063-z>.
- [7] T.-H. Wu, Y. Zhang, Z.D. Althouse, N. Liu, Nanoscale design of zinc anodes for high-energy aqueous rechargeable batteries, *Mater. Today Nano.* 6 (2019) 100032, <https://doi.org/10.1016/j.mtnano.2019.100032>.
- [8] Y. Li, H. Dai, Recent advances in Zinc-air batteries, *Chem. Soc. Rev.* 43 (2014) 5257–5275, <https://doi.org/10.1039/c4cs00015c>.
- [9] J. Zhang, Q. Zhou, Y. Tang, L. Zhang, Y. Li, Zinc-air batteries: are they ready for prime time? *Chem. Sci.* 10 (2019) 8924–8929, <https://doi.org/10.1039/C9SC04221K>.
- [10] Z. Zhou, Y. Zhang, P. Chen, Y. Wu, H. Yang, H. Ding, Y. Zhang, Z. Wang, X. Du, N. Liu, Graphene oxide-modified zinc anode for rechargeable aqueous batteries, *Chem. Eng. Sci.* 194 (2019) 142–147, <https://doi.org/10.1016/j.ces.2018.06.048>.
- [11] P. Chen, Y. Wu, Y. Zhang, T.-H. Wu, Y. Ma, C. Pelkowski, H. Yang, Y. Zhang, X. Hu, N. Liu, A deeply rechargeable zinc anode with pomegranate-inspired nanostructure for high-energy aqueous batteries, *J. Mater. Chem. A.* 6 (2018) 21933–21940, <https://doi.org/10.1039/C8TA07809B>.
- [12] J.F. Parker, C.N. Chervin, I.R. Pala, M. Machler, M.F. Burz, J.W. Long, D.R. Rolison, Rechargeable nickel-3D zinc batteries: an energy-dense, safer alternative to lithium-ion, *Science* 356 (2017) 415–418, <https://doi.org/10.1126/science.aak9991>.

- [13] Y. Yan, Y. Zhang, Y. Wu, Z. Wang, A. Mathur, H. Yang, P. Chen, S. Nair, N. Liu, A lasagna-inspired nanoscale ZnO anode design for high-energy rechargeable aqueous batteries, *ACS Appl. Energy Mater.* 1 (2018) 6345–6351, <https://doi.org/10.1021/acs.aem.8b01321>.
- [14] S.-M. Lee, Y.-J. Kim, S.-W. Eom, N.-S. Choi, K.-W. Kim, S.-B. Cho, Improvement in self-discharge of Zn anode by applying surface modification for Zn–air batteries with high energy density, *J. Power Sources* 227 (2013) 177–184, <https://doi.org/10.1016/j.jpowsour.2012.11.046>.
- [15] Y.-D. Cho, G.T.-K. Fey, Surface treatment of zinc anodes to improve discharge capacity and suppress hydrogen gas evolution, *J. Power Sources* 184 (2008) 610–616, <https://doi.org/10.1016/j.jpowsour.2008.04.081>.
- [16] M. Yano, S. Fujitani, K. Nishio, Y. Akai, M. Kurimura, Effect of additives in zinc alloy powder on suppressing hydrogen evolution, *J. Power Sources* 74 (1998) 129–134, [https://doi.org/10.1016/S0378-7753\(98\)00044-5](https://doi.org/10.1016/S0378-7753(98)00044-5).
- [17] Z. Zhang, Z. Yang, J. Huang, Z. Feng, X. Xie, Enhancement of electrochemical performance with Zn–Al–Bi layered hydrotalcites as anode material for Zn/Ni secondary battery, *Electrochim. Acta* 155 (2015) 61–68, <https://doi.org/10.1016/j.electacta.2014.12.145>.
- [18] Y.-J. Li, L. Cui, P.-F. Da, K.-W. Qiu, W.-J. Qin, W.-B. Hu, X.-W. Du, K. Davey, T. Ling, S.-Z. Qiao, Multiscale structural engineering of Ni-doped CoO nanosheets for zinc–air batteries with high power density, *Adv. Mater.* 30 (2018) 1804653, <https://doi.org/10.1002/adma.201804653>.
- [19] M.J. Tan, B. Li, P. Chee, X. Ge, Z. Liu, Y. Zong, X.J. Loh, Acrylamide-derived freestanding polymer gel electrolyte for flexible metal–air batteries, *J. Power Sources* 400 (2018) 566–571, <https://doi.org/10.1016/j.jpowsour.2018.08.066>.
- [20] H.-J. Lee, J.-M. Lim, H.-W. Kim, S.-H. Jeong, S.-W. Eom, Y.T. Hong, S.-Y. Lee, Electrospun polyetherimide nanofiber mat-reinforced, permselective polyvinyl alcohol composite separator membranes: a membrane-driven step closer toward rechargeable zinc–air batteries, *J. Membr. Sci.* 499 (2016) 526–537, <https://doi.org/10.1016/j.memsci.2015.10.038>.
- [21] J. Meng, F. Liu, Z. Yan, F. Cheng, F. Li, J. Chen, Spent alkaline battery-derived manganese oxides as efficient oxygen electrocatalysts for Zn–air batteries, *Inorg. Chem. Front.* 5 (2018) 2167–2173, <https://doi.org/10.1039/C8QI00404H>.
- [22] H. Li, Q. Li, P. Wen, T.B. Williams, S. Adhikari, C. Dun, C. Lu, D. Itanze, L. Jiang, D. L. Carroll, G.L. Donati, P.M. Lundin, Y. Qiu, S.M. Geyer, Colloidal cobalt phosphide nanocrystals as trifunctional electrocatalysts for overall water splitting powered by a zinc–air battery, *Adv. Mater.* 30 (2018) 1705796, <https://doi.org/10.1002/adma.201705796>.
- [23] B. Li, J. Chai, X. Ge, T. An, P. Lim, Z. Liu, Y. Zong, Sheet-on-Sheet hierarchical nanostructured C@MnO<sub>2</sub> for Zn–air and Zn–MnO<sub>2</sub> batteries, *ChemNanoMat* 3 (2017) 401–405, <https://doi.org/10.1002/cnma.201700043>.
- [24] B. Li, J. Quan, A. Loh, J. Chai, Y. Chen, C. Tan, X. Ge, T.S.A. Hor, Z. Liu, H. Zhang, Y. Zong, A robust hybrid Zn–battery with ultralong cycle life, *Nano Lett.* 17 (2017) 156–163, <https://doi.org/10.1021/acs.nanolett.6b03691>.
- [25] W. Niu, Z. Li, K. Marcus, L. Zhou, Y. Li, R. Ye, K. Liang, Y. Yang, Surface-modified porous carbon nitride composites as highly efficient electrocatalyst for Zn–air batteries, *Adv. Energy Mater.* 8 (2018) 1701642, <https://doi.org/10.1002/aenm.201701642>.
- [26] P. Bonnicks, J.R. Dahn, A simple coin cell design for testing rechargeable zinc–air or alkaline battery systems, *J. Electrochem. Soc.* 159 (2012) A981–A989, <https://doi.org/10.1149/2.023207jes>.
- [27] S. Dongmo, J.J.A. Kreissl, K. Miyazaki, T. Abe, T.-H. You, C.-C. Hu, D. Schröder, Reproducible and stable cycling performance data on secondary zinc oxygen batteries, *Sci. Data* 7 (2020) 395, <https://doi.org/10.1038/s41597-020-00728-3>.
- [28] J. Nan, D. Han, M. Yang, M. Cui, Dismantling, recovery, and reuse of spent nickel–metal hydride batteries, *J. Electrochem. Soc.* 153 (2006) A101, <https://doi.org/10.1149/1.2133721>.
- [29] J.M. Olivares-Ramírez, M.L. Campos-Cornelio, J. Uribe Godínez, E. Borja-Arco, R. H. Castellanos, Studies on the hydrogen evolution reaction on different stainless steels, *Int. J. Hydrogen Energy* 32 (2007) 3170–3173, <https://doi.org/10.1016/j.ijhydene.2006.03.017>.
- [30] S.A.S. Machado, L.A. Avaca, The hydrogen evolution reaction on nickel surfaces stabilized by H-absorption, *Electrochim. Acta* 39 (1994) 1385–1391, [https://doi.org/10.1016/0013-4686\(94\)E0003-1](https://doi.org/10.1016/0013-4686(94)E0003-1).
- [31] J.M. Costa, J.R. Culleré, The effect of additives on the corrosion of tin in alkaline solution, *Corrosion Sci.* 16 (1976) 587–590, [https://doi.org/10.1016/S0010-938X\(76\)80017-0](https://doi.org/10.1016/S0010-938X(76)80017-0).
- [32] Y. Wu, Y. Zhang, Y. Ma, J.D. Howe, H. Yang, P. Chen, S. Aluri, N. Liu, Ion-sieving carbon nanoshells for deeply rechargeable Zn-based aqueous batteries, *Adv. Energy Mater.* 8 (2018) 1802470, <https://doi.org/10.1002/aenm.201802470>.
- [33] Y. Zhang, Y. Wu, H. Ding, Y. Yan, Z. Zhou, Y. Ding, N. Liu, Sealing ZnO nanorods for deeply rechargeable high-energy aqueous battery anodes, *Nano Energy* 53 (2018) 666–674, <https://doi.org/10.1016/j.nanoen.2018.09.021>.
- [34] M.B. Lim, T.N. Lambert, E.I. Ruiz, Effect of ZnO-saturated electrolyte on rechargeable alkaline zinc batteries at increased depth-of-discharge, *J. Electrochem. Soc.* 167 (2020), 060508, <https://doi.org/10.1149/1945-7111/ab7e90>.
- [35] Y. Wu, P.-W. Huang, J.D. Howe, Y. Yan, J. Martinez, A. Marianchuk, Y. Zhang, H. Chen, N. Liu, Operando visualization of the electrochemical formation of liquid polybromide microdroplets, *Angew. Chem. Int. Ed.* (2019), <https://doi.org/10.1002/anie.201906980>.
- [36] Y. Zhang, Y. Wu, W. You, M. Tian, P.-W. Huang, Y. Zhang, Z. Sun, Y. Ma, T. Hao, N. Liu, Deeply rechargeable and hydrogen-evolution-suppressing zinc anode in alkaline aqueous electrolyte, *Nano Lett.* 20 (2020) 4700–4707, <https://doi.org/10.1021/acs.nanolett.0c01776>.